# Origin of the Bathochromic Shift of Astaxanthin in Lobster Protein: 2D Electronic Spectroscopy Investigation of beta-Crustacyanin

Christensson, Niklas; Zidek, Karel; Magdaong, Nikki Cecil M.; LaFountain, Amy M.; Frank, Harry A.; Zigmantas, Donatas

*Published in:*
The Journal of Physical Chemistry Part B

*DOI:*
10.1021/jp401873k

2013

*Document Version:*
Peer reviewed version (aka post-print)

# The Origin of the Bathochromic Shift of Astaxanthin in Lobster Protein: 2D Electronic Spectroscopy Investigation of $\beta$-crustacyanin

Niklas Christensson,[†,§] Karel Žídek,[‡,§] Nikki Cecil M. Magdaong,[¶] Amy M. LaFountain,[¶] Harry A. Frank,[¶] and Donatas Zigmantas[*,‡]

*Faculty of Physics, University of Vienna, Strudlhofgasse 4, 1090 Vienna, Austria, Department of Chemical Physics, Lund University, Box 124, 21000, Lund, Sweden, and Department of Chemistry, University of Connecticut, Storrs, Connecticut 06269-3060, USA*

E-mail: Donatas.Zigmantas@chemphys.lu.se

KEYWORDS: $\beta$-crustocyanin, astaxanthin, two-dimensional electronic spectroscopy, ultrafast spectroscopy, bathochromic shift, exciton-vibrational model

[*]To whom correspondence should be addressed
[†]Faculty of Physics, University of Vienna, Strudlhofgasse 4, 1090 Vienna, Austria
[‡]Department of Chemical Physics, Lund University, Box 124, 21000, Lund, Sweden
[¶]Department of Chemistry, University of Connecticut, Storrs, Connecticut 06269-3060, USA
[§]Contributed equally to this work

**Abstract**

We report on ultrafast spectroscopy study of $\beta$-crustacyanin - the carotenoprotein responsible for the coloration of the lobster shell. $\beta$-crustacyanin is formed by two closely positioned astaxanthin molecules encapsulated in protein. The two-dimensional (2D) electronic spectroscopy together with two-color pump-probe were applied to investigate the electronic structure, excited state dynamics and the influence of the excitonic interaction between the two carotenoids in $\beta$-crustacyanin.

By using the ~ 20 fs laser pulses tuned to absorption bands of the $S_0$-$S_2$ and $S_1$-$S_n$ transitions of carotenoids we were able to trace full excitation relaxation dynamics, starting with $S_2$ - $S_1$ relaxation on the ~30 fs timescale and finishing with the ground state recovery of 3.2 ps. Superimposed on the relaxation dynamics in the 2D spectra we observed long-lived beating signals at the characteristic frequencies of astaxanthin vibrational modes. We assign these oscillations to the ground-state vibrational wavepacket dynamics.

All features of the 2D spectra, including amplitude and phase maps of the long-lived oscillations, were reproduced by employing exciton-vibronic model. Consistent modeling of all optical properties of $\beta$-crustacyanin (including absorption and circular dichroism spectra) points to the relatively weak coupling between the two astaxanthin molecules (~ 250 $cm^{-1}$). This implies that the excitonic coupling provides insignificant contribution to the bathochromic shift in $\beta$-crustacyanin. We discuss the origin of the shift and propose that it is caused by two major effects: conformational changes of astaxanthin molecules (increase in effective conjugation length) together with increased charge transfer character of the $S_2$ state. We put the bathochromic shift in the broad perspective of other "blue" carotenoids properties.

# Introduction

$\beta$-crustacyanin ($\beta$-Cr) counts among the most studied carotenoproteins owing to its unique and intriguing optical properties.[1–6] It is the basic building block of the pigment protein complex $\alpha$-crustacyanin ($\alpha$-Cr), which is responsible for the coloration of lobsters and other blue-black crustaceans. X-ray crystalography investigations have revealed that $\beta$-Cr binds two astaxanthin (AXT)

molecules at a minimum inter-molecular distance of 7 Å.[2] Upon binding to the protein, the absorption maximum shifts from 480-490 nm for the carotenoids in solution to approximately ~580 nm, corresponding to a bathochromic shift of 4000 $cm^{-1}$(Figure1).[1] In nature, $\beta$-Crs aggregate into an octamer named $\alpha$-Cr, which has absorption shifted even further to 630 nm..

A number of theoretical and experimental studies have addressed the issue of the bathochromic shift in $\beta$-Cr and the mechanism of coloration of the crustaceans.[1–6] However, biochemical and some quantum chemical investigations favor distinctly different explanations for the shift. The proposed mechanisms can be divided into three groups.

The first mechanism is the resonance coupling between the two AXT molecules in $\beta$-Cr. The coupling is mediated by both large transition dipole moments of the carotenoids as well as by the small inter-molecular distance, which results in a redistribution of the energies of the excited states. Simple calculations based on the dipole-dipole interaction approximation supported this view and predicted a bathochromic shift of about 4000 $cm^{-1}$.[5] However, such simplified calculations are known to overestimate resonance coupling when inter-molecular distance is comparable to the size of the molecules.[7] Calculations employing more advanced methods did not confirm this result and predicted a more moderate coupling of 250 $cm^{-1}$.[4,8] Furthermore, assignment of a significant influence of the excitonic coupling to the bathochromic shift is in disagreement with the observation of shifts of similar magnitude in asteriarubin, a caroteno-protein binding a single carotenoid, and also contradicts the extensive reconstitution studies.[1] Similar conclusions can be drawn from the experiments on aggregated AXTs lacking the spectral shift,[9] effectively demonstrating that a short inter-molecular distance cannot alone be the explanation for the observed bathochromic shift.

The second mechanism involves site-specific interactions with the protein takes place in $\beta$-Cr. For instance the shift is conditioned by the presence of the $C_4$ carbonyl groups (see Figure1),[1] which can undergo an additional protonation by histidine residues in protein.[1,4] However, the experimental study of $^{13}$C-labeled AXT molecules by using nuclear magnetic resonance brought evidence against strong protonation of the carbonyl groups.[5]

Third, AXT in $\beta$-Cr adopts a different conformation compared to solution. The end rings of

AXT in $\beta$-Cr become almost co-planar with the conjugated chain, which increases the effective conjugation length.[2] Nevertheless, the increase in effective conjugation length cannot be the only explanation for the bathochromic shift, as even one of the longest carotenoids (M19, $N_{eff}$=17) does not appear blue in solution.[10]

Besides the insight into the origin of the crustaceans coloration, $\beta$-Cr provides an excellent model system for studies of the interaction between closely positioned carotenoid found in photosynthetic protein-pigment complexes and in artificial carotenoid aggregates.[11] Of particular interest is the peridinin-chlorophyll-protein (PCP) complex, where the carotenoid-carotenoid distances vary in the rage of 4-11 Å and the role of interaction between carotenoids on funneling the energy towards chlorophylls remains unexplored.[12]

In this work we employed two-dimensional electronic spectroscopy (2DES) in combination with two-color pump-probe to investigate the excited state dynamics and electronic structure of $\beta$-Cr. 2DES has proven to be a powerful tool for disentangling dynamics in complicated molecular systems,[13,14] and can provide valuable information about inter-molecular couplings and system-bath interaction. By virtue of the combination of high time resolution (~20 fs) 2DES and pump-probe techniques we were able to capture the energy relaxation between the $S_2$ and $S_1$ states manifold. Superimposed on the system relaxation in the 2D spectra we observed clear signatures of ground state vibrational wavepackets dynamics and analyze the corresponding amplitude and phase maps in detail.

We present a model highlighting the interplay of resonance coupling between AXTs and the high frequency vibrational modes characteristic of carotenoids, which provides a unified description of linear absorption, circular dichroism (CD) as well as 2DES and pump-probe results. On the basis of these results we conclude that the resonance interaction between the carotenoid makes a minor contribution to the bathochromic shift in $\beta$-Cr. In the end, we discuss other major contributions to the bathochromic shift as conformational change and carotenoid-protein interactions, where AXT stucture (specific interactions) as well as general properties of carotenoids (non-specific interactions) play important roles.

# Experimental

## Sample preparation

$\beta$-Cr was extracted from the carapace of an American lobster (Homarus americanus) according to the protocol of Zagalsky.[15,16] Unless otherwise stated, all preparations were done in the cold and under low light. One large (~1 kg) lobster was sacrificed by deep-freezing at -20ºC, and the carapace was removed and scrubbed under cold water to remove the hypodermis and other uncalcified parts. The cleaned carapace was left to dry overnight in a cold room at 4 ºC, after which time all parts of the shell were broken into small pieces and ground in a grinder, using ~10 sec bursts to avoid heating the sample.

The ground pieces were then sieved through a brass U.S.A. standard test sieve (30 mesh per inch) and transferred immediately to 4 L of Tris-borate buffer comprised of 0.3 M boric acid adjusted to pH 6.8 using solid Tris (Fisher Scientific). This mixture was then ground for 16 hours in the cold room using a rotary ball mill until it had a powder consistency. A foamy suspension was also present in the ball mill. Both the foamy suspension and the powdered material were filtered on a Büchner funnel layered with Hyflo* SuperCel* Filter Aid (Fisher Scientific) and washed with Tris-borate buffer followed by water.

The protein was extracted by resuspending the dry cake from the Büchner filtration step in 5 L of a 10% EDTA pH 7.5 aqueous solution. The mixture was stirred overnight then filtered through a layer of filter aid. The dark blue filtrate was then stored in a freezer at -20ºC while the dry cake was extracted again by stirring in 5 L of EDTA solution for another 48 hours. All of the blue filtrates were then combined, and the pH was adjusted to 7.5 using 2 M HCl.

The pigment-protein complexes were precipitated using solid ammonium sulfate to 50% saturation (313 g/L), filtered twice on a Büchner funnel layered with filter aid and redissolved in 0.2 M potassium phosphate buffer at pH 7. The precipitation of impurities was achieved by bringing the solution to 30% ammonium sulfate saturation (176 g/L) and centrifuging the sample for 30 min at 20000 g in a Sorvall RC-5B superspeed centrifuge using an SS34 rotor. The supernatant was

removed and adjusted to 50% ammonium sulfate saturation and stored at 4ºC. Subsequently, the sample was centrifuged at 20000 g for 30 min in a Sorvall RC-5B superspeed centrifuge using an SS34 rotor and the precipitate containing the pigment-protein complexes was dissolved in 50 mM potassium phosphate buffer at pH 7. The ammonium sulfate concentration was reduced by dialysis against the same buffer for 24 hours.

Column chromatography was performed to separate $\beta$-Cr (purple fraction) from the $\alpha$-Cr and $\delta$-Cr (blue fractions). The solution was loaded onto a DEAE-cellulose (Sigma-Aldrich, catalog number D-6418) column (2.4 cm i.d., 10 cm length) prior-equilibrated by washing with 0.5 M and subsequently 50 mM potassium phosphate buffer at pH 7. $\beta$-Cr (purple eluate) passed directly through the column upon elution with the 50 mM potassium phosphate buffer and was collected and stored in a solution containing 60% saturated ammonium sulfate. The blue fraction containing $\alpha$-Cr and $\delta$-Cr as well as residual $\beta$-Cr was collected by gradient elution using 0-1.0 M KCl in 50 mM potassium phosphate buffer. The components of the blue fraction were further separated by stepwise elution on another DEAE-cellulose column using 0.050 M, 0.150 M and 0.250 M phosphate buffer at pH 7 which eluted $\beta$-Cr, $\delta$-Cr and $\alpha$-Cr, respectively.

All purified protein samples were adjusted to 50% saturated ammonium sulfate and stored in the freezer at -20ºC until ready for use.

## Two-dimensional electronic spectroscopy

2DES measurements were carried out on a double modulation lock-in detection setup.[17] Yb:KGW amplified laser system (Pharos, Light Conversion) working at repetition rate of 20 kHz was used to pump a home-built non-collinear optical parametric amplifier (NOPA). By using the NOPA, infrared laser pulses (1030 nm) were converted into visible region (590 nm, bandwidth of ~60 nm) with a pulse duration of 15 fs. The generated visible pulses were divided into four beams of equal intensity by a beam splitter (beams 1,2 and 3,4) and a transmission grating (1 – 2, and 3 – 4) with delays introduced by a delay line (population time, $t_2$) and fused silica wedges (coherence time, $t_1$). Finally, beams were focused in the boxcar geometry to overlap in the sample. Beam 4 (the

local oscillator, LO) arrived ~ 1 ps in advance and was attenuated approximately 1000 times. In order to extract 2DES signal from the scattering of pump pulses, beams 1 and 2 were modulated by two phase-locked optical choppers running at frequency ratio of 3/7. Interferograms of the 2DES signal and the LO pulse were continuously read out by the CCD camera and signals modulated at both sum and difference frequencies of the choppers were recorded. 2D spectra were collected by scanning the coherence time $t_1$ from - 48 fs to 48 fs with a step of 0.8 fs. The real part of the 2D spectra was obtained by phasing corresponding 2D spectrum projection to the spectrally resolved pump-probe signal.[18]

The pump-probe experiments were carried out on the same experimental setup. Beams 1 and 3 were blocked, while beams 2 and three times attenuated 4 were used as pump and probe pulses, respectively. Beams 2 and 4 were each modulated by optical choppers and the probe spectrum was detected by the CCD and recorded on the sum and difference frequencies of the choppers. Two-color pump-probe measurements were carried out by using one NOPA (Light Conversion) to generate the excitation wavelength of 590 nm, (bandwidth of 50 nm, pulse duration of 20 fs) and a second NOPA (home-built) to generate the probe wavelength of 765 nm, (bandwidth of 95 nm, pulse duration of 14 fs). The pump and probe pulses passed through the setup in the identical way as in the single-color experiment.

All experiments were carried out at room temperature. No change in $\beta$-Cr absorption during measurements was observed. The sample was driven by a peristaltic pump through the 0.2 mm optical path flow cell (0.2 mm thin quartz windows) and optical density of the sample was kept at about 0.1.

# Vibronic-exciton model

## Electronic structure and linear spectroscopy

Linear and nonlinear spectra of carotenoids are strongly influenced by the presence of the two strong intra-molecular vibrational modes corresponding to the C-C ($f_2$) and C=C ($f_1$) vibrations

of the polyene chain. For AXT, additional strong coupling to the bath, as well as disorder of the terminal rings, erases the vibrational structure typically seen for linear carotenoids. The linear- and nonlinear-response of carotenoids have previously been modeled using the lineshape function approach[19–21], which is able to treat arbitrary coupling between electronic and nuclear degrees of freedom exactly. In the present case, the additional resonance coupling between the carotenoids will lead to a mixing of the vibrational manifolds of the two monomers in the excited state. Rather than attempting a perturbative expansion in the excitonic coupling,[22] we introduce the two strongest vibrational modes directly into the system Hamiltonian together with the electronic resonance coupling. After diagonalization, we obtain vibronic-exciton states, which represent mixed vibrational and electronic states of the two molecules in the dimer.[23] The residual intra- and inter-molecular nuclear modes are treated as a thermal heat bath giving rise to coherence and population dynamics on the vibronic-exciton eigenstates of the system. The results presented below is a straightforward generalization of the single-mode results discussed in a number of recent publications.[24–26]

The Hamiltonian of the system, including the two carotenoids together with the vibronic manifold of the two vibrational modes, is written as

$$H_S = \sum_{n,\mathbf{q_e}} \left[E_n - E_b + \mathbf{f}\cdot\mathbf{q_e}\right] |n,\mathbf{q_e}\rangle\langle n,\mathbf{q_e}| + J_0 \sum_{n,\mathbf{q_e}}\sum_{m,\mathbf{q'_e}} (1-\delta_{n,m})\, \langle \mathbf{q_e}|\mathbf{0}\rangle\langle \mathbf{q'_e}|\mathbf{0}\rangle |n,\mathbf{q_e}\rangle\langle m,\mathbf{q'_e}|, \qquad (1)$$

where the vectors $\mathbf{f} = [f_1, f_2]$ and $\mathbf{q_e} = [q_1, q_2]$ denote the vibrational frequencies and the quantum numbers in the excited state of the two vibrational modes, respectively. $J_0$ is the electronic resonance coupling and the brackets denote the Frank-Condon amplitudes. $E_n$ is the energy of the AXT monomer and $E_b$ is the bathochromic shift (see discussion below). The eigenvalues of $H_S$ are given by $E_\alpha = \hbar\omega_\alpha$ and the eigenstates of the system are expressed using the monomeric combined electronic/vibrational states and the expansion coefficients $c_{n,\mathbf{q_e}}$ as

$$|\alpha\rangle = \sum_{n,\mathbf{q_e}} c_{n,\mathbf{q_e}} |n,\mathbf{q_e}\rangle. \qquad (2)$$

The transition dipole moment from the electronic ground state with the vibrational quantum numbers $\mathbf{q_g}$ to an eigenstate $|\alpha\rangle$ in the first vibronic exciton manifold is given by

$$\mu_{\alpha\lambda} = \sum_{n,\mathbf{q_e}} c_{n,\mathbf{q_e}} \mathbf{d}_n \langle \mathbf{q_e} | \mathbf{q_g} \rangle, \tag{3}$$

where $d_n$ denotes the monomer electronic transition dipole moment vector. $\lambda = 2\pi \sum \mathbf{q_g} - \mathbf{0}$ denotes the energy of the vibrational configuration in the ground state, where we have adopted the short hand notation $[0,0] \equiv \mathbf{0}$.

The two vibrational modes have high frequencies and will not be populated at room temperature. To calculate the linear absorption spectrum, we can thus safely assume that only vibrational ground state is initially populated. Within this approximation, the linear absorption spectrum is given by

$$OD(\omega) = \Re \left\langle \sum_{\alpha} \int_0^{\infty} \mu_{\alpha \mathbf{0}}^{\mathbf{2}} e^{-g_{\alpha\alpha}(t) - \Gamma_\alpha t} e^{i(\omega_{\alpha 0} + \omega)t} dt \right\rangle_{\Delta}, \tag{4}$$

where $g_{\alpha\alpha}(t)$ is the lineshape function in the eigenstate representation[25,27] and $\Gamma_\alpha$ is the population relaxation rate of state $\alpha$. $\langle \rangle_\Delta$ denotes average over the inhomogeneous distribution of pigment transition energies. The circular dichroism spectrum (CD) is calculated in a similar fashion using the rotation strength $r_{\alpha 0}$ instead of $\mu_{\alpha 0}^2$ .[28] The rotation strength is given by

$$r_{\alpha 0} = \sum_{n,\mathbf{q_e} < m,\mathbf{q'_e}} c_{n,\mathbf{q_e}} c_{m,\mathbf{q'_e}} \langle \mathbf{q_e} | \mathbf{0} \rangle \langle \mathbf{q'_e} | \mathbf{0} \rangle \mathbf{R}_{nm} \cdot (\mu_{\mathbf{n}} \times \mu_{\mathbf{m}}), \tag{5}$$

where $\mathbf{R}_{nm}$is the displacement vector between the two electronic transition dipoles $\mu_{\mathbf{n}}$ and $\mu_{\mathbf{m}}$, and $\times$ denotes the vector cross-product.

The electronic coupling between the AXT molecules in $\beta$-Cr has been the subject of intensive debate with theoretically predicted values ranging from 250 to 4000 cm$^{-1}$.[5,6,8] Due to the close proximity of the carotenoids, this value can not be estimated with the dipole-dipole approximation, and in this work we will use the value from quantum chemical calculations on the complete dimer[6,8] corresponding to $J_0 = 250$ cm$^{-1}$. This coupling strength is much less than the width

of the (linear) absorption spectrum of the monomer, indicating that the average eigenstates in the dimer will be similar to those in the isolated monomers. We therefore introduce the approximation $g_{\alpha\alpha}(t) = g(t)$ in eq 4.

Furthermore, this localization implies that population relaxation between the vibronic states in the first exciton manifold is slow due to the small vibronic-exciton overlaps (see equation 3 in Ref. 25) and will be similar to the vibrational relaxation rate in the monomer. Therefore in the following we will assume that the population relaxation rate is dominated by relaxation from the $S_2$ to the $S_1$ manifold. The final approximation thus amounts to the substitution $\Gamma_\alpha = \Gamma$ in eq 4 , where we use $\Gamma = \frac{1}{30}\,\mathrm{fs}^{-1}$ obtained from the pump-probe kinetics (see next section). These two approximations are also employed for the calculation of the 2D spectrum.

The frequencies of the two strong vibrational modes in carotenoids have been studied by a number of techniques. Here we use typical values for carotenoids with an effective conjugation length of 11;[29] $f_2 = 1155\ \mathrm{cm}^{-1}$ and $f_1 = 1520\ \mathrm{cm}^{-1}$ corresponding to the C-C and C=C vibrations and set the Huang-Rhys factors of both modes to 0.6. Resonance Raman spectroscopy has shown that the $f_2$ mode gains in intensity and that the $f_1$ mode shifts down in frequency (20 $\mathrm{cm}^{-1}$) upon binding of AXT to the protein.[1,5] These effects are beyond the simple model presented here and we will keep the frequencies the same as for the monomers. The large Huang-Rhys factors of the two vibrational modes implies that a large number of vibrational states needs to be explicitly included in the Hamiltonian. Here we include all vibrational states with maximum 6 quanta in each mode giving in total 72 vibronic-exciton states in the dimer.

The nuclear modes not treated explicitly give rise to dephasing via the lineshape function in eq 4. The lineshape function is determined by the cosine transform of the spectral density reflecting the density of states of these modes weighted by the coupling strength of each mode.[27] The spectral density for AXT in solution has been determined by three-pulse photon echoes in Ref. 19 . However, unlike in Ref. 19 we treat the "slow" modes as a true inhomogeneous broadening (explicit averaging over disorder). We keep the ratio of "fast" to "slow" nuclear motions as estimated in Christensson et al.,[19] and use a total reorganization energy of 1000 $\mathrm{cm}^{-1}$ and a disorder ($\Delta$) of

1250 $cm^{-1}$ (FWHM).

## Two-dimensional spectra

The 2DES and pump-probe experiments, as shown below, revealed that the excited state lifetime in $\beta$-Cr is very short ($\sim$30 fs). The short excited state lifetime, in combination with the absence of significant changes to the 2D lineshapes for $t_2$>100 fs, indicates that the 2D spectra measured after $t_2$=100 fs can be modeled in the Markov approximation and the Liouville pathways propagating in the excited state state during $t_2$ can be ignored. The relevant Liouville pathways contributing to the ground state bleach (GSB) signal are illustrated by the Feynman diagrams in Figure 7. In the Markov approximation, we can express these pathways via the transition dipole moments and the Greens function propagators as[26]

$$R^{NR}_{\alpha\beta,\lambda} = \left\langle \mu_{\alpha 0}\mu_{\alpha\lambda}\mu_{\beta\lambda}\mu_{\beta 0} G_{\alpha 0}(t_1)\, G^{(2)}_{\lambda}(t_2)\, G_{\beta 0}(t_3) \right\rangle_{\Omega\Delta}, \tag{6}$$

$$R^{R}_{\alpha\beta,\lambda} = \left\langle \mu_{\alpha 0}\mu_{\alpha\lambda}\mu_{\beta 0}\mu_{\beta\lambda} G^{*}_{\alpha 0}(t_1)\, G^{(2)*}_{\lambda}(t_2)\, G_{\beta\lambda}(t_3) \right\rangle_{\Omega\Delta},$$

where $\alpha\beta$ represent the labels of the involved excited states and $\lambda$ is the frequency difference between *bra* and *ket* sides after two interactions (i.e. 0, $f_1$ or $f_2$). The Greens function propagators are given by $G_{\alpha\lambda}(t) = e^{(-i\omega_{\alpha\lambda}t - \Gamma t - g(t))}$ and $G^{(2)}_{\lambda}(t) = e^{-i\lambda t}$ and the star (*) denotes complex conjugation. The brackets denote average of the involved transition dipole moments over a random distribution of orientations ($\Omega$) and pigment energies ($\Delta$). To calculate the 2D spectrum we evaluate the double Fourier transform of the rephasing and nonrephasing pathways in eq 6. For the non-rephasing pulse order

$$S_{NR}(\omega_1, t_2, \omega_3) = \sum_{\alpha\beta,\lambda} A^{NR}_{\lambda}(\omega_1,\omega_3)\, R^{NR}_{\alpha\beta,\lambda}(\omega_1,\omega_3)\, e^{-i\lambda t_2}, \tag{7}$$

where $A^{NR}_{\lambda}(\omega_1,\omega_3)$ is an amplitude factor reflecting the magnitude of the electric field $E$ at

the frequencies of interactions for the particular Liouville pathway. From the Feynman diagrams shown in Figure 7 we can write

$$A_{\lambda}^{R}(\omega_1,\omega_3) = E(\omega_1)E(\omega_1-\lambda)E(\omega_3), \tag{8}$$

$$A_{\lambda}^{NR}(\omega_1,\omega_3) = E(\omega_1)E(\omega_1-\lambda)E(\omega_3-\lambda). \tag{9}$$

For $\lambda = 0$, we recover the time independent GSB contribution. The square root of the laser spectrum in Figure 1 was used as the electric field in the calculations.

# Results and Discussion

## Linear Spectra

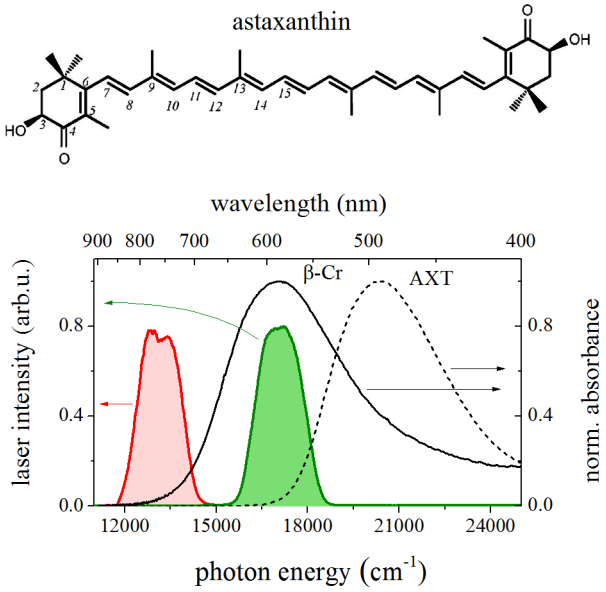


Figure 1: Upper panel: chemical structure of astaxanthin molecule. Lower panel: absorption spectra of astaxanthin molecules in chloroform (dashed line) and in $\beta$-Cr (solid line); spectra of the laser pulses used to study $S_0$-$S_2$ absorption region (filled green area) and $S_1$-$S_n$ excited state absorption region (filled pink area).

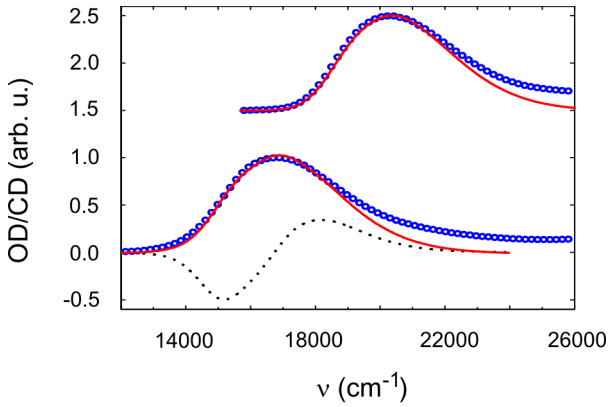


Figure 2: Linear absorption spectrum of astaxanthin in chloroform and in $\beta$-Cr (blue circles) together with a fit discussed in the text (red line). Also shown is the simulated CD spectrum based on the model (dotted line).

AXT in chloroform displays a featureless broad spectrum typical for carotenoids having carbonyl groups on the terminal rings (see Figure 1).[30,31] The absorption maximum shifts from 20350 $cm^{-1}$ (491 nm) to 17080 $cm^{-1}$ (585 nm) when two AXTs are bound to the protein and form $\beta$-Cr. Figure 2 shows the simulations of the linear absorption spectra of both the AXT monomer in solution and $\beta$-Cr together with the measured spectra. For the simulation of the linear spectrum of AXT we used an $S_2$ lifetime of 160 fs,[3] and a bathochromic shift of $E_b = 3650$ $cm^{-1}$ was subtracted from the transition energy in order to reproduce the absorption maximum of $\beta$-Cr.

We also present the simulated CD spectrum of $\beta$-Cr, which shows a characteristic doublet structure with the negative feature at lower frequencies. The splitting between the negative peak and the zero crossing is 1500 $cm^{-1}$, which is very close to the experimental value.[1] This demonstrates that the large splitting seen in the CD spectrum is consistent with the moderate resonance coupling.[4,8] Unlike the experimental CD spectrum, the negative peak in the simulated CD spectrum is stronger than the positive one. We point out that asteriarubin, a protein which only binds a single carotenoid, shows a positive CD signal which roughly follows the linear absorption spectrum and which has a similar magnitude to that of $\beta$-Cr[1]. This implies that the carotenoids themselves gives a contribution to the CD spectrum. Such effects are not included in our model where the CD signal vanish when the resonance coupling approaches zero.

The difficulties of obtaining a qualitative match to the entire CD spectrum, as well as the broad

lineshapes, makes it problematic to determine the upper bound on the resonance coupling. To illustrate the effect of resonance coupling on the linear spectra we performed the calculations for the resonance coupling of 500 $cm^{-1}$. This value leads to a blue shift of the linear absorption spectrum by 250 $cm^{-1}$, an increase of the width of the spectrum by 400 $cm^{-1}$, and an increase of the splitting in the CD spectrum to 1650 $cm^{-1}$. For the resonance coupling above 1250 $cm^{-1}$we observe a clear splitting of the linear spectra into two components where the feature at high frequency is stronger, compared to the low-frequency one.

Thus we conclude that a coupling larger than 1000 $cm^{-1}$ is not consistent with the linear spectroscopy data and the large splitting found in the CD spectrum does not originate from large excitonic coupling, but results from very broad lineshapes and high density of vibronic-exciton states. The weak coupling in comparison to the linewidths shows that the electronic states in $\beta$-Cr are largely monomeric in nature and we will therefore in the remaining sections use standard notation for the carotenoid excited states.

## Excited state dynamics

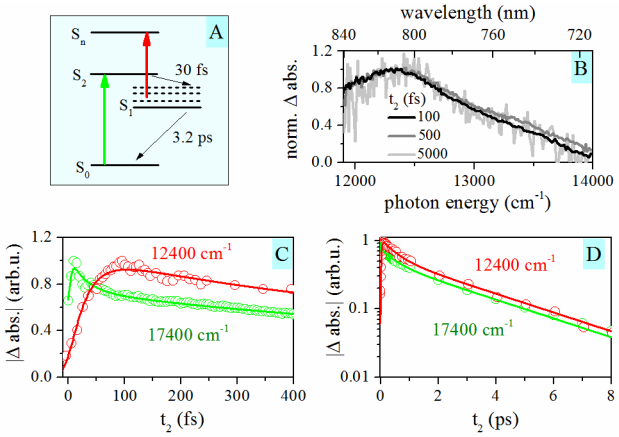


Figure 3: (A) Scheme of the energy states and dynamics in $\beta$-Cr (green and red arrows – photon energies of laser pulses, black arrows – relaxation processes). (B) Normalized transient absorption spectra for several pump-probe delays ($t_2$) indicated in the legend. Fast (C) and slow (D) dynamics of pump-probe signal (red open circles) and integrated 2DES signal (green open circles) fitted by a three-exponential function (solid lines, see text for details).

We will first turn to the excited state dynamics in $\beta$-Cr, which we investigated by using pump-

probe experiments tuned to the $S_0$-$S_2$ and $S_1$-$S_n$ transitions (see Figure 3 A). The transient absorption spectra in the NIR region depicted in Figure 3 B revealed a broad excited state absorption (ESA) band, which can be assigned to the $S_1$-$S_n$ transition. Maximum of the band (12400 $cm^{-1}$) is shifted by 5000 $cm^{-1}$ compared to the absorption maximum, which is similar to the shift observed for $\alpha$-Cr (shift of 4200 $cm^{-1}$).[3] As the shape of the spectrum did not change with $t_2$, we will focus here exclusively on the kinetics of the signal maximum.

The kinetic trace at 12400 $cm^{-1}$, shown in Figure 3 C and D, exhibit a sub-100 fs rise followed by a slow decay on a picosecond timescale. At the same time, kinetics in the GSB region exhibit a sub-100 fs decay followed by the relaxation on a ps timescale.

It is possible to fit the kinetics at 12400 and 17400 $cm^{-1}$ by a three-exponential function convoluted with experimental setup response function (Gaussian function with FWHM of 20 fs). Three components feature lifetimes of 30 fs, 500 fs and 3.2 ps – see Table 1 for details and Figure 3A for the model of the electronic structure with assigned relaxation processes.

**Table 1: Fitting parameters obtained by the simultaneous fit of signal kinetics in Figure 3 C and D by a three-exponential function convoluted with the Gaussian function (experimental setup response function, FWHM 20 fs).**

| $\nu_{probe}$ ($cm^{-1}$) | $\tau_1$ (fs) | $A_1$ (%) | $\tau_2$ (fs) | $A_2$ (%) | $\tau_3$ (fs) | $A_3$ (%) |
|---|---|---|---|---|---|---|
| 17400 | 30 | 30 | 500 | 25 | 3200 | 45 |
| 12400 | | -100 | | 45 | | 55 |

The slowest component, 3.2 ps, reflects the ground state recovery and is manifested as a decay in both the GSB and in the ESA signals. Interestingly, there is a striking correlation between AXT absorption band position (20800 $cm^{-1}$ in solvent, 17100 $cm^{-1}$ in $\beta$-Cr, and 15900 $cm^{-1}$ in $\alpha$-Cr) and the $S_1$ lifetimes (5 ps, 3.2 ps, and 1.8 ps, respectively).[3] The $S_1$ lifetime in carotenoids is known to correlate with the effective conjugation length.[11] For instance, carotenoid 3´-hydroxyechinenone (3HEN) has an $S_1$ lifetime of 6.5 ps in solution, which decreases to 3.3 ps when the carotenoid is bound in the orange carotenoid protein.[32] Based on the crystal structure, it was concluded that the reduction of the $S_1$ lifetime resulted from a planarization of the end-rings in the binding pocket.

In the case of $\beta$-Cr and $\alpha$-Cr, this would imply that additional planarization takes place upon aggregation of the $\beta$-Cr subunits. However, the crystal structure of $\beta$-Cr shows that end-rings are almost perfectly planar already in $\beta$-Cr[2] and it is difficult to envision that further planarization of the carotenoids could be responsible for the large change in the $S_1$ lifetime between $\beta$-Cr and $\alpha$-Cr. Nonetheless, resonance Raman experiments have shown that the frequency of the $f_1$ vibration is lower in $\alpha$-Cr than in $\beta$-Cr,[5] indicating a further extension of the effective conjugation length[29] in agreement with the decrease of the $S_1$ lifetime. However, the change of the $f_1$ frequency is rather small and it is unlikely that increasing the effective conjugation length is alone responsible for the large reduction of the $S_1$ lifetime. Other interactions may be important in this case.[33]

The intermediate component, with a 500 fs time constant, is more difficult to assign. Ilagan et al.[3] observed a similar decay component in $\alpha$-Cr and assigned it to vibrational relaxation in the $S_1$ manifold. We find that this component is present in both $S_1$-$S_n$ ESA as well as in the GSB signal which makes an assignment similar to vibrational relaxation unlikely. Without more information about the spectrum of this component, a decisive assignment is not possible because it could in principle reflect a general decay of the signal due to system-bath interactions.

The fastest component manifest itself as a decay in the $S_0$-$S_2$ signal and, at the same time, as a rise in the $S_1$-$S_n$ ESA . Therefore we assign the 30 fs component to relaxation from the $S_2$ to $S_1$ manifold. This relaxation time is about 5 times faster than the corresponding one for the carotenoid in solution,[3] but quite similar to the value obtained for short chain carotenoids,[34] where the $S_2$-$S_1$ relaxation time is about 45 fs due to a reduced $S_2$- $S_1$ energy gap. If we use the $S_1$ lifetime to obtain a (rough) estimate of the $S_1$ energy, we obtain a shift of $\sim$400 cm$^{-1}$compared to solution. On the other hand, the $S_2$ energy shifts by $\sim$4000 cm$^{-1}$. This leads to a reduction in the $S_2$- $S_1$ energy gap down to a value which is similar to that observed for the short chain carotenoids.[34]

## Two-dimensional Spectra

Further insight into the $\beta$-Cr dynamics can be obtained by employing the 2DES measurements. The 2D spectrum of $\beta$-Cr is featureless with a rectangular shape, which does not change signifi-

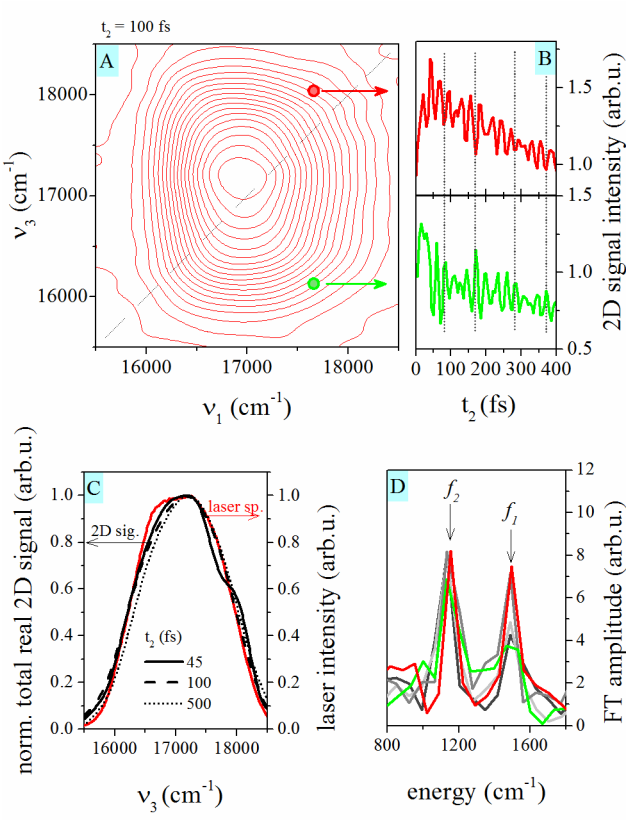


Figure 4: (A) The real part of the 2D spectrum of $\beta$-Cr at population time of 100 fs. (B) Signal dynamics in population time for two different spectral regions ($\nu_1$= 17660 cm$^{-1}$; red: $\nu_3$ = 18140 cm$^{-1}$; green:$\nu_3$ = 16230 cm$^{-1}$ ) with a pronounced out off phase oscillation pattern. Dotted lines serve as guides to the eye. (C) Normalized real part of the 2D spectra of $\beta$-Cr for $\nu_1$= 17200 cm$^{-1}$ at various populations times (black lines) compared to the used laser spectrum (red line). (D) FT amplitude of the 2DES population time kinetics presented on panel (B) (red and green line) and for other spectral positions in the 2D spectrum (gray lines).

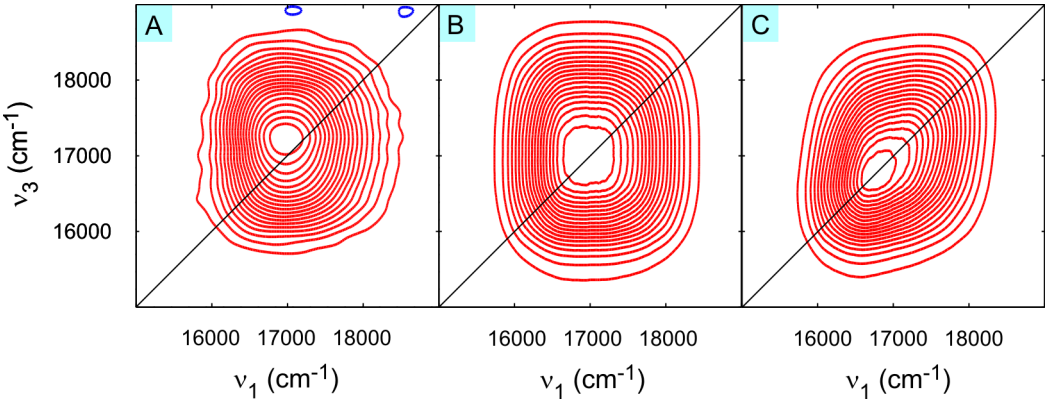


Figure 5: A) Experimental 2D spectrum of $\beta$-Cr at 1 ps . B) Simulation of the stationary ground state bleach contribution. C) Simulation of the stationary ground state bleach contribution without the cross-peak contributions. Contour lines are drawn in 5 % intervals starting from 5 %.

cantly for $t_2 > 100$ fs, only decays with the ground state recovery time of 3.2 ps (see Figure 4A). The fact that the absorption band of $\beta$-Cr significantly exceeds the used laser spectrum (see Figure 1), has a significant impact on the observed lineshapes, which follows laser spectrum profile. This is illustrated in Figure 4C, which compares the 2DES signal cut along the $\nu_3$ axis and the laser spectrum.

The experimentally obtained 2D spectra can be readily reproduced by the presented exciton-vibronic model, as it is illustrated in Figure **5** comparing the simulated GSB contribution with the experimental 2D spectrum at $t_2 = 1$ ps. Both the simulated and experimental spectra have a rectangular shape, which is slightly more elongated along the $\nu_3$ axis. This elongation can be understood from the amplitude factors in eq 8 and 9, which bring about an asymmetric distortion of the 2D spectrum. Traditionally, large anti-diagonal width is taken as an indication of a largely homogeneous transition.[35] Thus the square shape of the spectrum points to the transition that is largely homogeneously broadened. Indeed, the large coupling to the bath in the case of carotenoids together with the short $S_2$ life-time gives rise to a large homogeneous broadening. On the other hand, the lack of vibrational structure in the linear absorption spectrum of the monomer and in $\beta$-Cr indicates that the system has significant inhomogeneity. Our theoretical treatment based on vibronic-exciton eigenstates provides the explanation for the shape of the spectrum. The square shape has its origin in the large number of overlapping cross-peaks resulting from transitions to all vibronic-exciton states in the excited state manifold. Figure **5** illustrates the influence of these cross-peak contributions by comparing the simulation including all possible pathways with the simulation including "diagonal" contribution only (i.e. $R = R_{\alpha\beta}\delta_{\alpha\alpha}$). Neglecting the cross-peak contributions results in a 2D spectrum, which is more elongated along the diagonal and reflects the inhomogeneity of the system. However, including all contributions is required to recover the characteristic shape of the experimental spectrum.

Population time evolution analysis of the 2D spectrum reveals long-lived oscillations (see Figure 4B), which decay only on a picosecond timescale. As it is evident from Figure 4B, the oscillations barely decay during the first 400 fs. A Fourier transform (FT) maps of the 2DES signal

dynamics (Figure 4D) revealed two modes with frequencies of ~ 1500 $cm^{-1}$ (mode $f_1$) and ~ 1150 $cm^{-1}$ (mode $f_2$). These wavenumbers correspond to the two dominant vibrational modes of the polyenic chain in AXT: the C-C and C-H in plane bending ($f_2$ = 1155-1158 $cm^{-1}$), and the C=C stretching vibrations ($f_1$ = 1498-1520 $cm^{-1}$).[5,36] Based on the similarities to the known frequencies of vibrational modes in AXT and on the observation that the oscillations' lifetime greatly exceeds the lifetime of the excited state, we assign them to the vibrational wavepacket dynamics in the ground state.

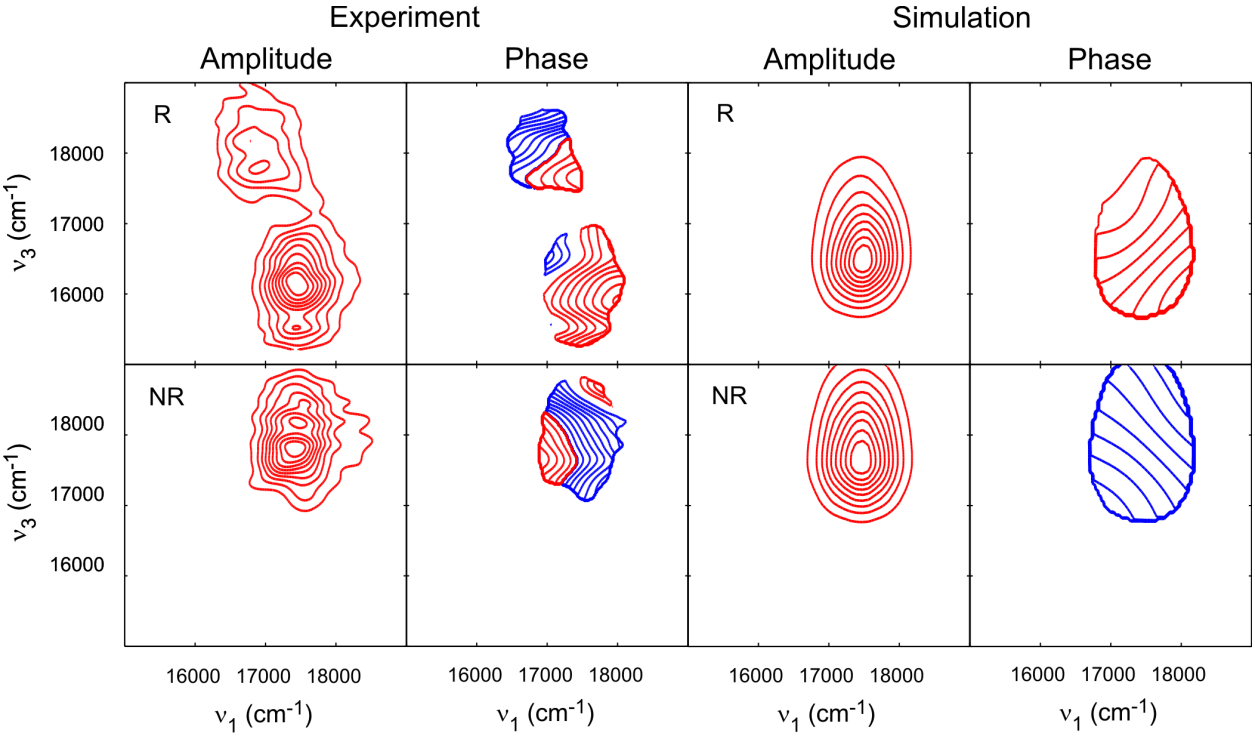


Figure 6: FT amplitude and phase maps of the oscillations in $\beta$-crustacyanin of the $f_2 = 1150$ $cm^{-1}$ mode. Contour lines are drawn in 10 % intervals starting from 10 %. Negative values in the phase maps are shown as blue lines. Left side of the figure shows the experimental results and the right side the results of the model discussed in the text.

To analyze the oscillations further, amplitude and phase maps were generated from a FT over $t_2$ for a 45×45 grid of $\nu_1$ and $\nu_3$ values in the 2D spectrum. The amplitude and phase maps for rephasing and non-rephasing pulse order for the $f_2$ vibration at 1150 $cm^{-1}$ are shown in Figure 6. Analysis of the $f_1$ mode revealed qualitatively similar results and will not be discussed further.

Starting with the amplitude maps, we find that a significant oscillation amplitude is only ob-

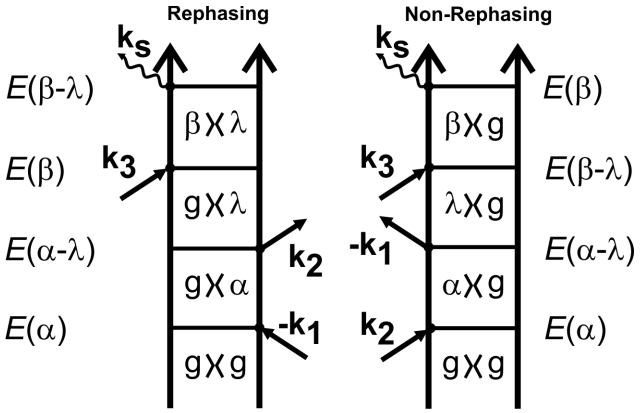


Figure 7: Double-sided Feynman diagrams for the ground state bleaching pathways.

served above $\nu_1$ =17000 cm$^{-1}$. The appearance of the amplitude maps can be understood from the rephasing (R) and non-rephasing (NR) Feynman diagrams shown in Figure 7 and from the amplitude factors in eq 8 and 9. First, the second term in eq 8 and 9 shows that if the first interaction has a low frequency, it will not be possible to excite the vibrational level in the ground electronic state with the second interaction. Therefore no oscillation amplitude at low $\nu_1$ can be detected. The difference between R and NR pulse order is manifested during the last two interactions. For R pathways, the emission (4:th interaction, curved arrow) does not return the system to the vibrational ground state but to a vibrational excited state. The maximum in the amplitude map will thus be found at $\nu_3 \approx \nu_1 - \lambda$. For the NR pathways, the third interaction interacts with the excited vibrational mode in the ground state. Such excitation will preferentially lead to emission at $\nu_3 \approx \nu_1$, because the states at lower energy are effectively discriminated against by the lack of spectral amplitude at lower frequencies.

The phase maps do not have such an intuitive explanation as the amplitude maps. The phase of the oscillation is determined by the product of the transition dipole moments.[37] In the case of a monomer, this product can be recast in terms of the relevant Frank-Condon amplitudes and depending on the quantum numbers of the involved states, the pathway can have either a positive or negative sign.[38,39] However, when realistic lineshapes are included, the phase will vary with the detuning from resonance.[39] In the dimer model we have a large number of pathways contributing to the signal. Furthermore, we average over disorder meaning that a point in the 2D spectrum does

not correspond to a well defined detuning (or well defined phase).

For vibronic excitons, the mixing of different vibronic transitions in the excited state manifold leads to further complications in the interpretation. In the present case, the mixing between the two monomers is rather weak due to the strong influence of the vibrational modes and the large inhomogeneous broadening. In fact, we find that the amplitude and phase maps look qualitatively similar when the electronic coupling is set to zero. This confirms the conclusion from the preceding section that the electronic states can be considered as largely monomeric in $\beta$-Cr.

The simple model outlined above is capable of explaining both the non-oscillating and oscillating contributions to the 2D spectrum quite well. A complication in the analysis is the broad bandwidth of $\beta$-Cr compared to the laser pulses. The finite bandwidth of the pulses limits the information that can be extracted from the spectrum. Here we have adopted a very simple approach where the simulations are carried out in the impulsive limit and the effect of the finite bandwidth on the time-independent and coherent pathways are accounted for by scaling the amplitude of each pathway by the electric fields of the involved interactions. This simple procedure is clearly sufficient to understand the spectra. However, the limitation of the approach can be seen in Figure 5, where the simulated spectrum is noticeably wider than the experimental one and the splitting between the peaks in the R and NR amplitude maps is underestimated (see Figure 6). These differences are related to the neglect of phase of the electric fields and the pulse overlap effects[40] Furthermore in experimental R amplitude map additional low amplitude peak at high $\nu_3$ frequencies is observed, whereas it is completely missing in corresponding simulated map. At the moment we do not have an interpretation of this feature. We can only speculate about the origin of discrepancies, but note that signatures of vibrational modes in coherent spectroscopy respond sensitively to small amounts of chirp of the excitation pulses.[40]

## Bathochromic shifts in $\beta$- and $\alpha$-crustacyanin

The discussion in the preceding sections have largely confirmed the findings from several recent quantum chemical studies suggesting a weak electronic coupling in $\beta$-Cr.[4,6] We can conclude that

the linear spectrum and the CD spectrum of $\beta$-Cr can be accounted for by a model with a moderate resonance interaction between the carotenoids. The resonance interaction does not lead to any significant shifts of the absorption maximum, and as pointed out by Neugebauer,[6] it actually shifts the spectrum somewhat to the blue. To reach an agreement with the experimental spectrum, we introduced a parameter $E_b$ to account for the bathochromic shift. To this point we have treated $E_b$ as a free parameter and in the following we discuss the different contributions to $E_b$ and try to estimate their magnitudes.

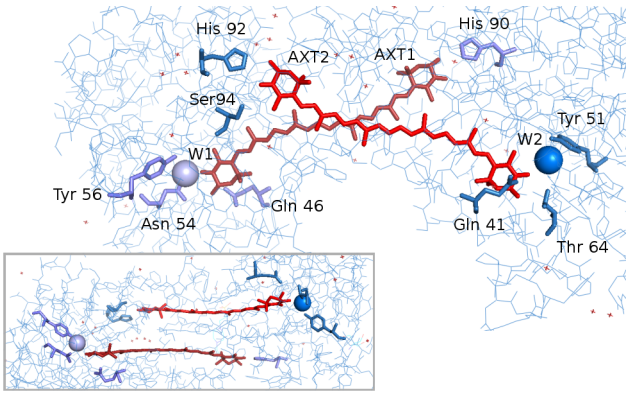


Figure 8: Structure of $\beta$-Cr illustrating interaction of the AXT dimer shown in red with protein environment (thin lines): top view (main figure) and side view (bottom left panel). Residues (thick lines) and water molecules (spheres) important for interaction between AXTs and protein are highlighted.[4]Other water molecules are denoted as red crosses.

First we will turn to AXT conformation changes. In solution, AXT adopts an s-cis conformation where the $\beta$-iodene rings are twisted with respect to the polyenic chain. The $S_1$ lifetime in solution is 5 ps, which corresponds to an effective conjugation length of ~10.5-11, implying that the central polyene chain contributes to the effective conjugation length.[3] Upon binding in $\beta$-Cr, the terminal rings planarize (see the side view of $\beta$-Cr in Figure 8) and the carotenoid adopts an s-trans conformation.[2] The $S_1$ lifetime drops to about 3 ps, indicative of a conjugation length of 11.5-12. In this configuration, the carbon bonds on the terminal rings are fully conjugated (s-trans). Based on these effective conjugation lengths, we can estimate that the $S_2$ energy drops approximately 600-1000 $cm^{-1}$.[11,41] The role of planarization can be directly evaluated by comparing AXT to cathaxanthin analogues where the 18 methyl group was removed to minimize steric interaction

and to favor a s-trans configuration. This procedure resulted in a shift of the linear absorption from 486 to 512 nm ( 1000 $cm^{-1}$).[42] Thus, a red shift of approximately 1000 $cm^{-1}$ seems to be a good estimate of the effect of increased conjugation in $\beta$-Cr. We note that this value is in a good agreement with quantum chemical calculations based on the crystal structure.[5,6] Turning to $\alpha$-Cr, both the red-shift of the $f_1$ vibration as well as the decrease of the $S_1$ lifetime indicates further extension of the effective conjugation. Because the conjugated system in $\beta$-Cr already comprise the carbons on the terminal rings, we conclude that further extension of the conjugation must involve the $C_4$-keto carbonyls. However, by comparing linear carotenoids with 12 and 14 conjugated bonds we can conclude that such an increase in conjugation only decreases the $S_2$ energy by a few hundred wavenumbers (~300 $cm^{-1}$) and can not be responsible for the difference between $\alpha$-Cr and $\beta$-Cr.[11,34]

An important factor for the bathochromic shift is a change in polarizability upon excitation of carotenoids resulting from the large (extended) conjugated system. For conjugated polyenes, the polarizability of a state is related to the bond length alternation (BLA), where a low (high) BLA leads to high (low) values of the polarizability.[43,44] States with $A_g$ symmetry (i.e. the covalent states $S_0$ and $S_1$) display a high degree of BLA as compared to $B_u$ states (i.e. the ionic states $S_2$ and $S_n$), giving rise to a large polarizability difference upon transition from $S_0$ to $S_2$ (and from $S_1$ to $S_n$). This effect is manifested as a large sensitivity of the $S_0$-$S_2$ transition energy to solvent polarizability or refractive index. For instance, the $S_0$-$S_2$ transition of astaxanthin shifts by 1200 $cm^{-1}$ between n-hexane (refractive index 1.375) and $CS_2$ (refractive index 1.63).[45].

The polarizability change upon excitation for AXT in solution and AXT bound in $\alpha$-Cr has been investigated by Stark spectroscopy.[36] It was shown that upon binding to the protein, the polarizability change ($\Delta\alpha$) increased by 50% and the dipole moment difference ($\Delta\mu$) doubled. Studies on different carotenoids in solutions[46] and in proteins[47] have demonstrated that $\Delta\alpha$ correlates with the conjugation length. Thus, the observed increase in $\Delta\alpha$ seems to be related to the conformational change upon binding as evident from the decrease in $S_1$ lifetime and the down-shift of the $f_1$ vibration. The increase in $\Delta\alpha$ revealed by the Stark experiments implies that bound carotenoids

are even more sensitive to dispersive interactions than the carotenoid in solution.

To estimate the spectral shift of AXT between solution (n-hexane) and the Cr environment, we assume that the dielectric properties of the protein can be approximated by pyridine. Its optical dielectric constant of 2.25 is in line with common values for the optical dielectric constant of proteins (2-2.1) and results in a reasonable estimate of the protein induced shift for other carotenoproteins (700 out of 1000 $cm^{-1}$ in LH2 and 700 of 820 $cm^{-1}$ in LH1). However, unlike these carotenoids, AXT in Cr undergoes a significant conformational change upon binding to the protein and an effective increase in the conjugation length. This increase in conjugation length leads to an increase in $\Delta\alpha$ by 50%, as it was shown by Stark experiments. By using the difference between the absorption maxima for AXT in n-hexane and in pyridine (850 $cm^{-1}$),[45] we estimate the bathochromic shift due to the dielectric environment to be about 1200 $cm^{-1}$.

The two mechanisms discussed in the preceding sections are of a general nature and are to a certain extent of relevance to all carotenoids bound in proteins. For instance, 3HEN in orange carotenoid protein[32] also experiences a conformational change, which increases the effective conjugation length and leads to a red-shift due to both mechanisms discussed above. However, the $S_0$-$S_2$ transition in orange carotenoid protein only shifts by 1000 $cm^{-1}$. In the case of AXT in $\beta$-Cr, our estimates give a somewhat larger value (~2200 $cm^{-1}$), but it is nonetheless clear that these two mechanisms alone cannot account for the large bathochromic shifts found for $\beta$-Cr and $\alpha$-Cr. Clearly, what distinguishes $\beta$-Cr from the other carotenoproteins must be either a specific property of the AXTs, a specific AXT-protein interaction, or the combined influence of both.

Besides $\alpha$-Cr and $\beta$-Cr, other "blue" carotenoids exist in nature or have been artificially synthesized. One common feature of these "blue" carotenoids is that they all incorporate electron acceptors in the conjugated system.[1,48–50] The acceptor creates an electronic pull and a partial charge separation that affects states of different symmetry in different ways. States of $A_g$ symmetry has a high BLA and the largely confined charges will not be perturbed to a large extent. In $B_u$ states (i.e. $S_2$), the BLA is significantly less and the electrons are freer to move. For these states, a larger dipole will be formed. When the molecule is placed in a moderately polar environment

like the crustacyanin binding pocket (Figure 8), the partial charge separation due to the acceptor will thus result in a red-shift of the $S_0$-$S_2$ transition.[1] The effect of the acceptors strength on the $S_0$-$S_2$ energy gap has been demonstrated by Marder et al.[49] Increasing the acceptor strength gave rise to a large $\Delta\mu$ and red-shifts of thousands of $cm^{-1}$. Similar effects have been demonstrated for symmetrically substituted carotenoids - adding a second carbonyl to an s-trans analogue of cathaxanthin shifts the absorption maximum from 512 to 552 nm (1100 $cm^{-1}$).[42] Even more dramatic shifts have been observed when a sulfur atom is substituted into the place of the oxygen.[50]

However, unlike the red-shift of the $S_0$-$S_2$ transition induced by the incorporated acceptors described above, the electronic pull mechanism in $\beta$-Cr must be activated by the protein. Support for this idea can be found in the reconstitution study by Britton et al.[1] These experiments revealed that i) the carbonyls are essential for the large bathochromic shift, ii) conjugation must extend to the carbonyl groups iii) the carbonyls must be in the position 4 - a carbonyl located at 3, although completely conjugated like in rhodoxanthin, does not lead to a red-shift. This implies that the interaction between the carbonyls and specific amino acids (i.e. histidines: His 90 and His 92)[2] and water in the protein plays a decisive role. Important residues for the AXT-protein interaction are depicted in Figure 8.[4]

This discussion leads to a qualitative explanation for the mechanism responsible for the bathochromic shift in $\beta$-Cr. Upon binding to the protein, AXT is forced into a conformation where the rings are planar with the polyene chain. The planarization leads to an extension of the conjugation out to the $C_4$carbonyl groups. H-bonding of the carbonyls acts to increase their electron acceptor character, which serves to increase the electronic pull on the $\pi$-system.[51] This partial charge transfer (CT) character results in a red-shift of the $S_0$-$S_2$ transition analogue to other carotenoids with electron acceptors incorporated into the $\pi$-system. In order for the charge transfer mechanism to be operational, a conformational change bringing the carbonyls into the conjugated system is required. As soon as the carotenoid is removed from the binding pocket, the carotenoid returns to the cis- conformation and the carbonyls are no longer part of the conjugated $\pi$-system. This in turn explains that AXT does not exhibit any spectral shifts between protic and aprotic solvents and why

the position of the keto-carbonyls is critical for the formation of the large bathochromic shift .[45]

This mechanism connects bathochromic shift of the AXT within the $\beta$-Cr protein environment to the family of other "blue" carotenoid and indicates that there is a common mechanism behind all these observations. Furthermore, it offers a consistent explanation of both the reconstitution studies as well as the optical and Stark experiments discussed in the preceding sections. It is also likely that a similar mechanism is active in asteriarubin although this can not be confirmed due to the lack of structure of the protein.

Upon aggregation into $\alpha$-Cr, the absorption maximum shifts further to the red. From the decrease in the $S_1$ lifetime and the downshift of the $f_1$ frequency, we can conclude that the effective conjugation length increases. This can explain a part of the additional red-shift, but not the 1400 $cm^{-1}$ observed in the experiment. The lack of structure for $\alpha$-Cr makes it difficult to pin down the origin of this additional bathochromic shift. The CT mechanism discussed above will be sensitive to the environment surrounding the carbonyls and we can speculate that a compression of the binding pocket, leading to shorter hydrogen bonding distances, increases the strength of the CT interaction leading to even larger bathochromic shifts.

# Conclusions

Linear and nonlinear spectroscopic methods together with numerical modeling have been applied to investigate the electronic structure, excited state dynamics and the influence of the excitonic interaction between the two carotenoids in $\beta$-Cr. We find that the linear spectrum, circular dichroism, and 2D spectra are consistent with a weak coupling between the two carotenoids. Our estimation of the excitonic coupling is in good agreement with recent quantum chemical calculations. The strong coupling to the two main vibrational modes of the carotenoid, in addition to a significant inhomogeneity, leads to a weak mixing between the manifold of electronic/vibrational states of the two monomers. The states can thus be considered to be largely monomeric, which was confirmed by analysis of the wavepacket modulations seen in the 2D spectra.

The excited state dynamics in $\beta$-Cr involves a 30 fs deactivation of the initially populated $S_2$ state. This value if about 5 times faster than for the monomer in solution. This difference can be traced back to a decrease in the $S_2$-$S_1$ energy gap, which leads to the reduced relaxation time. The $S_1$ lifetime is found to be 3.2 ps, which places it in between the lifetimes found for the monomer in solution (5 ps) and in $\alpha$-Cr (1.8 ps).[3] The reduction in lifetime is the result of planarization of the end-rings and an increase of the effective conjugation length.

The effectively weak electronic coupling implies that the excitonic effect is not relevant for the bathochromic shift in $\beta$-Cr . Rather, the origin of the this shift can be traced to two connected effects. Upon binding to the protein, AXT planarizes and the effective conjugation length increases. This leads to a direct decrease of the $S_2$ energy due to increased conjugation and to an indirect decrease of the $S_2$ energy in the protein environment due to the increase in polarizability difference caused by the conformation change. The direct and indirect contribution to the red-shift resulting from the conformational change is estimated to account for approximately half of the bathochromic shift. The remaining shift is proposed to originate from a partial charge transfer character of the $S_2$ state due to an electronic pull from the carbonyls. This effect is enabled by the conformational change, which allows the carbonyls to couple to the $\pi$-conjugated system and is enhanced by hydrogen bonding of the carbonyls in the protein environment. The proposed model of electron accepting groups responsible for the bathochromic shifts connects AXT in the $\beta$-Cr environment to the other "blue" carotenoids where electron acceptors incorporated into the conjugated system results in dramatic changes of the absorption spectra.

## Acknowledgement

The work in Lund was supported by the Swedish Research Council and the Knut and Alice Wallenberg Foundation. NC was supported by Austrian Science Foundation (FWF) and OeAD. Work in the laboratory of HAF was supported by grants from the National Science Foundation (MCB-0913022) and the University of Connecticut Research Foundation.

## References


(1) Britton, G.; Weesie, R. J.; Askin, D.; Warburton, J. D.; GallardoGuerrero, L.; Jansen, F. J.; deGroot, H. J. M.; Lugtenburg, J.; Cornard, J. P.; Merlin, J. C. Carotenoid Blues: Structural Studies on Carotenoproteins. *Pure Appl. Chem.* **1997**, *69*, 2075–2084.

(2) Cianci, M.; Rizkallah, P. J.; Olczak, A.; Raftery, J.; Chayen, N. E.; Zagalsky, P. F.; Helliwell, J. R. The Molecular Basis of the Coloration Mechanism in Lobster Shell: Beta-Crustacyanin at 3.2-Angstrom Resolution. *Proc. Natl. Acad. Sci. USA* **2002**, *99*, 9795–9800.

(3) Ilagan, R. P.; Christensen, R. L.; Chapp, T. W.; Gibson, G. N.; Pascher, T.; Polivka, T.; Frank, H. A. Femtosecond Time-Resolved Absorption Spectroscopy of Astaxanthin in Solution and in Alpha-Crustacyanin. *J. Phys. Chem. A* **2005**, *109*, 3120–3127.

(4) Durbeej, B.; Eriksson, L. A. On the Bathochromic Shift of the Absorption by Astaxanthin in Crustacyanin: a Quantum Chemical Study. *Chem. Phys. Lett.* **2003**, *375*, 30–38.

(5) van Wijk, A. A. C.; Spaans, A.; Uzunbajakava, N.; Otto, C.; de Groot, H. J. M.; Lugtenburg, J.; Buda, F. Spectroscopy and Quantum Chemical Modeling Reveal a Predominant Contribution of Excitonic Interactions to the Bathochromic Shift in Alpha-Crustacyanin, the Blue Carotenoprotein in the Carapace of the Lobster Homarus Gammarus. *J. Am. Chem. Soc.* **2005**, *127*, 1438–1445.

(6) Neugebauer, J.; Veldstra, J.; Buda, F. Theoretical Spectroscopy of Astaxanthin in Crustacyanin Proteins: Absorption, Circular Dichroism, and Nuclear Magnetic Resonance. *J. Phys. Chem. B* **2011**, *115*, 3216–3225.

(7) Olsina, J.; Durchan, M.; Minofar, B.; Polivka, T.; Mancal, T. Absorption Spectra of Astaxanthin Aggregates. *arXiv: physics/1208.4958. arXiv.org e-Print archive. http://www.arxiv.org/abs/1208.4958 (accessed Feb 8, 2012).* **2012**,

(8) Strambi, A.; Durbeej, B. Excited-State Modeling of the Astaxanthin Dimer Predicts a Minor

Contribution from Exciton Coupling to the Bathochromic Shift in Crustacyanin. *J. Phys. Chem. B* **2009**, *113*, 5311–5317.

(9) Bartalucci, G.; Fisher, S.; Helliwell, J. R.; Helliwell, M.; Liaaen-Jensen, S.; Warren, J. E.; Wilkinson, J. X-ray Crystal Structures of Diacetates of 6-s-cis and 6-s-trans Astaxanthin and of 7,8-didehydroastaxanthin and 7,8,7 ',8 '-tetradehydroastaxanthin: Comparison with Free and Protein-Bound Astaxanthins. *Acta Crystallogr., Sect. B: Struct. Sci.* **2009**, *B65*, 238–247.

(10) Andersson, P. O.; Gillbro, T. Photophysics and Dynamics of the Lowest Excited Singlet State in Long Substituted Polyenes with Implications to the Very Long-Chain Limit. *J. Chem. Phys.* **1995**, *103*, 2509–2519.

(11) Polivka, T.; Sundstrom, V. Ultrafast Dynamics of Carotenoid Excited States - From Solution to Natural and Artificial Systems. *Chem. Rev.* **2004**, *104*, 2021–2071.

(12) Polivka, T.; Hiller, R. G.; Frank, H. A. Spectroscopy of the Peridinin-Chlorophyll-a Protein: Insight into Light-Harvesting Strategy of Marine Algae. *Arch. Biochem. Biophys.* **2007**, *458*, 111–120.

(13) Dostál, J.; Mančal, T.; Augulis, R.; Vácha, F.; Pšenčík, J.; Zigmantas, D. Two-Dimensional Electronic Spectroscopy Reveals Ultrafast Energy Diffusion in Chlorosomes. *J. Am. Chem. Soc.* **2012**, *134*, 11611–11617.

(14) Bixner, O.; Lukes, V.; Mančal, T.; Hauer, J.; Milota, F.; Fischer, M.; Pugliesi, I.; Bradler, M.; Schmid, W.; Riedle, E.; Kauffmann, H. F.; Christensson, N. Ultrafast Photo-Induced Charge Transfer Unveiled by Two-Dimensional Electronic Spectroscopy. *J. Chem. Phys.* **2012**, *136*, 204503.

(15) Zagalsky, P. F. Invertebrate Carotenoproteins. *Methods Enzymol.* **1985**, *111*, 216–47.

(16) Zagalsky, P. F. In *Carotenoids*; Britton, G., Liaaen-Jensen, S., Pfander, H., Eds.; Birkhäuser Verlag AG, 1995; Vol. 1A; p 287.

(17) Augulis, R.; Zigmantas, D. Two-Dimensional Electronic Spectroscopy with Double Modulation Lock-in Detection: Enhancement of Sensitivity and Noise Resistance. *Opt. Express* **2011**, *19*, 13126–13133.

(18) Jonas, D. M. Two-dimensional Femtosecond Spectroscopy. *Annu. Rev. Phys. Chem.* **2003**, *54*, 425–463.

(19) Christensson, N.; Polivka, T.; Yartsev, A.; Pullerits, T. Photon Echo Spectroscopy Reveals Structure-Dynamics Relationships in Carotenoids. *Phys. Rev. B* **2009**, *79*, 245118.

(20) Sugisaki, M.; Yanagi, K.; Cogdell, R. J.; Hashimoto, H. Unified Explanation for Linear and Nonlinear Optical Responses in Beta-Carotene: A sub-20-fs Degenerate Four-Wave Mixing Spectroscopic Study. *Phys. Rev. B* **2007**, *75*, 155110.

(21) Christensson, N.; Milota, F.; Nemeth, A.; Sperling, J.; Kauffmann, H. F.; Pullerits, T.; Hauer, J. Two-Dimensional Electronic Spectroscopy of Beta-Carotene. *J. Phys. Chem. B* **2009**, *113*, 16409–16419.

(22) Mančal, T.; Balevičius, V.; Valkunas, L. Decoherence in Weakly Coupled Excitonic Complexes. *J. Phys. Chem. A* **2011**, *115*, 3845–3858.

(23) Philpott, M. R. Theory of the Coupling of Electronic and Vibrational Excitations in Molecular Crystals and Helical Polymers. *J. Chem. Phys.* **1971**, *55*, 2039–2054.

(24) Polyutov, S.; Kuhn, O.; Pullerits, T. Exciton-Vibrational Coupling in Molecular Aggregates:Electronic Versus Vibronic Dimer. *Chem. Phys.* **2012**, *394*, 21–28.

(25) Christensson, N.; Kauffmann, H. F.; Pullerits, T.; Mancal, T. Origin of Long-Lived Coherences in Light-Harvesting Complexes. *J. Phys. Chem. B* **2012**, *116*, 7449–7454.

(26) Chenu, A.; Christensson, N.; Kauffmann, H. F.; Mančal, T. Vibronic- and Vibrational-Coherence Enhancement in 2D Spectra of Photosynthetic Complexes.

*arXiv:physics/1211.4397 arXiv.org e-Print archive http://arxiv.org/abs/1211.4397 (accessed Feb 9, 2012)* **2012**,

(27) Mukamel, S. *Principles of Nonlinear Optical Spectroscopy*; Oxford University Press: Oxford, 1995.

(28) Renger, T.; Marcus, R. On the Relation of Protein Dynamics and Exciton Relaxation in Pigment-Protein Complexes: An Estimation of the Spectral Density and a Theory for the Calculation of Optical Spectra. *J. Chem. Phys.* **2002**, *116*, 9997–10019.

(29) Merlin, J. C. Resonance Raman Analysis of Astaxanthin-Protein Complexes. *J. Raman Spectrosc.* **1987**, *18*, 519–523.

(30) Zigmantas, D.; Hiller, R. G.; Sharples, F. P.; Frank, H. A.; Sundstrom, V.; Polivka, T. Effect of a Conjugated Carbonyl Group on the Photophysical Properties of Carotenoids. *Phys. Chem. Chem. Phys.* **2004**, *6*, 3009–3016.

(31) Chabera, P.; Fuciman, M.; Hribek, P.; Polivka, T. Effect of Carotenoid Structure on Excited-State Dynamics of Carbonyl Carotenoids. *Phys. Chem. Chem. Phys.* **2009**, *11*, 8795–8803.

(32) Polivka, T.; Kerfeld, C. A.; Pascher, T.; Sundstrom, V. Spectroscopic Properties of the Carotenoid 3'-hydroxyechinenone in the Orange Carotenoid Protein from the Cyanobacterium Arthrospira Maxima. *Biochemistry* **2005**, *44*, 3994–4003.

(33) Chabera, P.; Fuciman, M.; Naqvi, K. R.; Polivka, T. Ultrafast Dynamics of Hydrophilic Carbonyl Carotenoids - Relation between Structure and Excited-State Properties in Polar Solvents. *Chem. Phys.* **2010**, *373*, 56–64.

(34) Kosumi, D.; Fujiwara, M.; Fujii, R.; Cogdell, R. J.; Hashimoto, H.; Yoshizawa, M. The Dependence of the Ultrafast Relaxation Kinetics of the S-2 and S-1 States in Beta-Carotene Homologs and Lycopene on Conjugation Length Studied by Femtosecond Time-Resolved Absorption and Kerr-Gate Fluorescence Spectroscopies. *J. Chem. Phys.* **2009**, *130*, 214506.

(35) Roberts, S. T.; Loparo, J. J.; Tokmakoff, A. Characterization of Spectral Diffusion from Two-Dimensional Line Shapes. *J. Chem. Phys.* **2006**, *125*, 084502.

(36) Krawczyk, S.; Britton, G. A Study of Protein-Carotenoid Interactions in the Astaxanthin-Protein Crustacyanin by Absorption and Stark Spectroscopy; Evidence for the Presence of Three Spectrally Distinct Species. *Biochim. Biophys. Acta* **2001**, *1544*, 301–310.

(37) Farrow, D. A.; Smith, E. R.; Qian, W.; Jonas, D. M. The Polarization Anisotropy of Vibrational Quantum Beats in Resonant Pump-Probe Experiments: Diagrammatic Calculations for Square Symmetric Molecules. *J. Chem. Phys.* **2008**, *129*, 174509.

(38) Mancal, T.; Christensson, N.; Lukes, V.; Milota, F.; Bixner, O.; Kauffmann, H. F.; Hauer, J. System-Dependent Signatures of Electronic and Vibrational Coherences in Electronic Two-Dimensional Spectra. *J. Phys. Chem. Lett.* **2012**, *3*, 1497–1502.

(39) Butkus, V.; Zigmantas, D.; Valkunas, L.; Abramavicius, D. Vibrational vs. Electronic Coherences in 2D Spectrum of Molecular Systems. *Chem. Phys. Lett.* **2012**, *545*, 40–43.

(40) Christensson, N.; Avlasevich, Y.; Mullen, A. Y. K.; Pascher, T.; Pullerits, T. Weakly Chirped Pulses in Frequency Resolved Coherent Spectroscopy. *J. Chem. Phys.* **2010**, *132*, 174508.

(41) Frank, H. A.; Desamero, R. Z. B.; Chynwat, V.; Gebhard, R.; van der Hoef, I.; Jansen, F. J.; Lugtenburg, J.; Gosztola, D.; Wasielewski, M. R. Spectroscopic Properties of Spheroidene Analogs Having Different Extents of p-Electron Conjugation. *J. Phys. Chem. A* **1997**, *101*, 149–157.

(42) Beutner, S.; Schaper, O. G. K.; Martin, H. D. Conventional and Specially Designed Carotenoids: Synthesis, Optical Properties and Conductivity. *Pure Appl. Chem.* **1994**, *66*, 955–962.

(43) Meyers, F.; Marder, S. R.; Pierce, B. M.; Bredas, J. L. Electric-Field Modulated Nonlinear-Optical Pproperties of donor-Acceptor polyenes - Sum-over-States Investigation of the Re-

lationship between Molecular Polarizabilities (alpha, beta, and gamma) and Bond-Length Alternation. *J. Am. Chem. Soc.* **1994**, *116*, 10703–10714.

(44) Fuß, W.; Haas, Y.; Zilberg, S. Twin States and Conical Intersections in Linear Polyenes. *Chem. Phys.* **2000**, *259*, 273–295.

(45) Buchwald, M.; Jencks, W. P. Optical Properties of Astaxanthin Solutions and Aggregates. *Biochemistry* **1968**, *7*, 834–843.

(46) Krawczyk, S.; Olszowka, D. Spectral Broadening and its Effect in Stark Spectra of Carotenoids. *Chem. Phys.* **2001**, *265*, 335–347.

(47) Nakagawa, K.; Suzuki, S.; Gardiner, R. F. A. T.; Cogdell, R. J.; Nango, M.; Hashimoto, H. Probing the Effect of the Binding Site on the Electrostatic Behavior of a Series of Carotenoids Reconstituted into the Light-Harvesting 1 Complex from Purple Photosynthetic Bacterium Rhodospirillum Rubrum Detected by Stark Spectroscopy. *J. Phys. Chem. B* **2008**, *112*, 9467–9475.

(48) Polivka, T.; Frank, H. A.; Enriquez, M. M.; Niedzwiedzki, D. M.; Liaaen-Jensen, S.; Hemming, J.; Helliwell, J. R.; Helliwell, M. X-ray Crystal Structure and Time-Resolved Spectroscopy of the Blue Carotenoid Violerythrin. *J. Phys. Chem. B* **2010**, *114*, 8760–8769.

(49) Marder, S. R.; Torruellas, W. E.; BlanchardDesce, M.; Ricci, V.; Stegeman, G. I.; Gilmour, S.; Bredas, J. L.; Li, J.; Bublitz, G. U.; Boxer, S. G. Large Molecular Third-Order Optical Nonlinearities in Polarized Carotenoids. *Science* **1997**, *276*, 1233–1236.

(50) Sliwka, H. R.; Liaaen-Jensen, S. Synthetic Sulphur Carotenoids.3. Carotienoid Thiones 1st Preparation and Spectroscopic Properties. *Acta Chem. Scand.* **1994**, *48*, 679–683.

(51) Zagalsky, P. F. $\beta$-Crustacyanin, the Blue-Purple Carotenoprotein of Lobster Carapace: Consideration of the Bathochromic Shift of the Protein-Bound Astaxanthin. *Acta Crystallogr., Sect. D: Biol. Crystallogr.* **2003**, *D59*, 1529–1531.

Table of Contents Figure: